Modeling of impedance of cell-covered electrodes

D.W. Greve and X. Huang
Dept. Electrical and Computer Engineering
Carnegie Mellon University
Pittsburgh, PA, USA
dg07@andrew.cmu.edu
xiaoqiu@andrew.cmu.edu

D. Nguyen and M.M. Domach
Department of Chemical Engineering
Carnegie Mellon University
Pittsburgh, PA, USA
dnguyen@andrew.cmu.edu
md0q@andrew.cmu.edu

Abstract

Measurements of the impedance of cell-covered electrodes can be used to detect the presence of cells, their motion, and can yield information about biological processes. In this paper we present the results of finite element modeling of the impedance of cell-covered electrodes. The emphasis is on the behavior of small electrodes comparable to the cell size.

Keywords

biosensor, impedance, electrodes, gold

INTRODUCTION

Previous work on the impedance of cell-covered electrodes has shown that important insights into biological processes can be obtained from electrical measurements. The first studies were reported by Giaever and coworkers who used electrode impedance measurements to monitor cell proliferation, morphology, and motility [1,2,3]. Their measurements were interpreted with the aid of theoretical calculations of the impedance changes caused by a disk-shaped cell on a large electrode [4]. In this work, the typical electrode size was substantially larger than the cells being studied (typically area ~ 5×10^{-4} cm^2). Other researchers have used impedance measurements to study cell monolayers [5] and the effect of toxic metals [6]. We are seeking to develop arrays of cell-sized electrodes which can be used in combinatorial biology and possibly for bioagent detection. This paper focuses on the understanding of the impedance changes resulting from cell growth on small electrodes.

ELECTRODE DESIGN AND IMPEDANCE WITHOUT CELLS

We seek to use an array of cell-sized metal electrodes to sense the motion and presence of cells in real time. A possible electrode design for this purpose is shown in Fig. 1. In this figure the sensing electrode is 30 μm square and is surrounded by a larger counterelectrode. Arrays presently in fabrication by our coworkers [7] have electrodes ranging in size from 30 to 40 μm square. Also shown in Fig. 1 is a tracing (to scale) of a mouse fibroblast growing on a culture plate surface. Typical cells will cover a large fraction of sensing electrodes of this size when centered over the electrode.

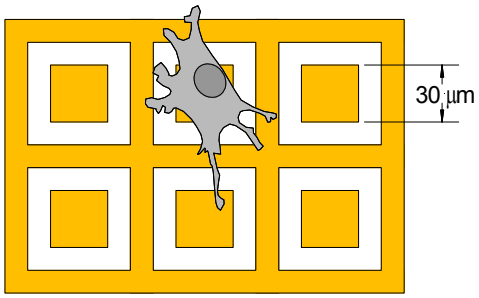

Figure 1. Array of sensing electrodes with large counterelectrode.

In this paper we seek to understand the effect of cell growth on the small-signal impedance of one of these electrodes. We first report on the results of finite element simulations of an idealized cell centerd on a single electrode. We will then show that more complex cases of realistic cell shapes and larger electrodes.

Electrode impedance measurements are performed with the electrodes immersed in cell growth medium, which has a large ion concentration and high electrical conductivity (0.015 $\Omega^{-1}cm^{-1}$). Ionic liquids form an electrical double layer at the interface between the liquid and metal electrodes. This electrical double layer is approximately 2 nm in thickness and consists of a compact or Helmholtz layer together with a diffuse layer approximately 2 nm in thickness. The electrical impedance of the electrical double layer varies with measurement frequency includes contributions both from the capacitance of the diffuse layer and also diffusive ionic transport.

Figure 2 shows measurements of the small signal impedance magnitude as a function of frequency for a gold electrodes immersed in cell growth medium. The impedance was measured between electrodes of varying area and a much larger counterelectrode.

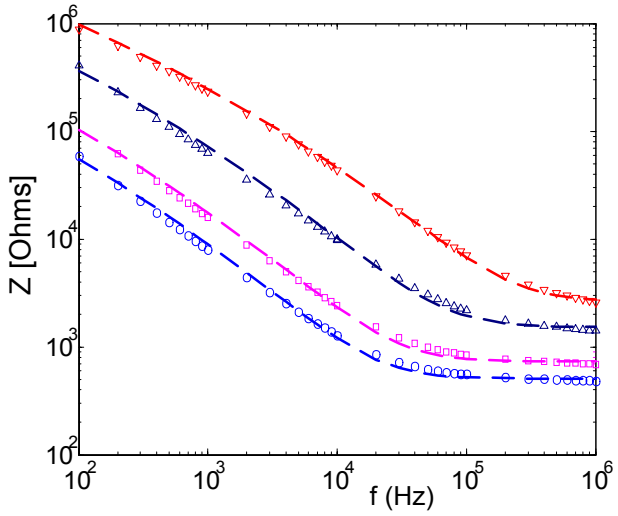

Figure 2. Measured impedance magnitude as a function of frequency for electrodes in cell growth medium: (○) 0.0032 cm^2 (□) 0.0016 cm^2 (△) 0.00032 cm^2, and (▽) 0.000064 cm^2 electrode area.

The measured impedance is proportional to f^n with $n \sim 0.67$ for low frequencies and becomes constant at high frequencies. A constant impedance is observed at high frequencies because the impedance of the electrical double layer becomes small compared to the spreading resistance in the cell growth medium. This behavior is modeled well by the equivalent circuit shown in Fig. 3, where Z_W represents the impedance associated with diffusive ion transport (Warburg impedance), C_I the capacitance of the electrical double layer, R_{ct} the charge transfer resistance, and R_S is the spreading resistance. In the case of our electrodes the measured impedance can be fit with $R_{ct} = 0$. Adopting the usual form for the Warburg or ion transport term [ ], the impedance becomes

$$Z(\omega) = \frac{1}{(s + js)A\omega^{1/2} + j\omega C_I A} + a\frac{\rho_m}{A^{1/2}}.$$

where s [sec$^{1/2}$/Ω·cm^2] and C_I [F/cm^2] are parameters which model the double-layer impedance.

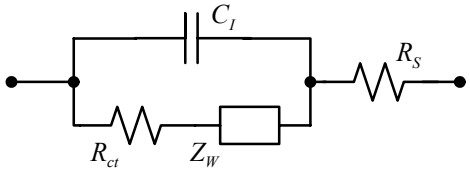

Figure 3. Equivalent circuit.

For purposes of simulation, we have adopted the values $s = 2.4 \times 10^{-4}$ sec$^{1/2}$/Ω·cm and $C_I = 15 \times 10^{-6}$ F/cm^2, which are chosen to be in reasonable agreement both with values extracted from our measurements and values in the literature.

Finite element simulations using the actual double layer thickness of a few nanometers would be impractical because the enormous difference in scale between the cell size and the double layer thickness would result in an impractically large number of elements. We address this by modeling the double layer thickness by a layer with a larger thickness t with dielectric permittivity ε_{dl} and conductivity σ_{dl} given by the expression

$$\sigma_{dl} + j2\pi f\varepsilon_{dl} = t\left[s\omega^{1/2} + js\omega^{1/2} + jC_I\omega\right].$$

The electrode simulated in this work had a size of 32 μm square and was separated from a surrounding counterelectrode by 9 μm. A model cell was centered on the sensing electrode. Because of symmetry, only one quarter of the electrodes were simulated. The electrodes and the domain used for simulation are shown in Fig. 4.

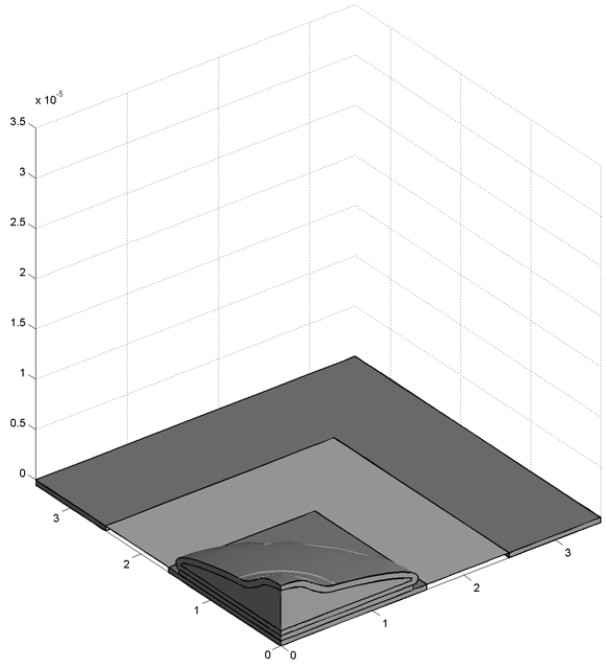

Figure 4. The simulation domain showing the sensing and counterelectrode and the centered cell.

SIMULATION OF IMPEDANCE WITH A CELL

Simulations of the electrode impedance with and without cells was performed using the three-dimensional DC conductivity mode of FEMLAB. In the DC conductivity mode it is possible to enter complex resistivities for the various regions and consequently an AC steady-state solution can be obtained [8].

Cells consist of a poorly conducting cell membrane approximately 8 nm in thickness representing a capacitance of about 10^{-6} F/cm^2. Conduction currents through this membrane due to ion channels have been neglected in this work as they become important only at lower measurement frequencies [9]. The cell interior is highly conducting and is modeled by a conductivity of 0.015 Ω^{-1}cm^{-1}. Cells make contact to surfaces by focal adhesion regions which repre-

sent a small fraction (15-20%) of the total cell area. Apart from the focal adhesion regions, there is a gap between the cell and the surface which ranges from 0.5 to 0.15 μm. In this work, we have considered cell-electrode gaps of 0.015 μm and 0.15 μm and the focal adhesion regions have been neglected in the simulations. As noted earlier, a wide range of scale makes finite element simulations difficult. We have therefore modeled the cell-electrode gap by a region of thickness 0.5 μm with conductivity increased to keep the sheet conductance unchanged. Similarly, the cell membrane thickness has been increased to 0.5 μm and the dielectric permittivity has been adjusted to give a capacitance of 10^{-6} F/cm^2 at the simulation frequency. In addition to making finite element simulations practical, these changes make it easier to visualize the results of the simulation.

Simulations were performed over the frequency range from 100 to 10^7 Hz. A voltage of $1 + j0$ volts was imposed on the sensing electrode and the counterelectrode was grounded. All other surfaces had an insulating boundary condition. The impedance magnitude was calculated by summing the current over the sensing electrode and forming the ratio

$$|Z| = \frac{1\ volt}{4 \cdot |I_{sensing}|}$$

Figure 5 shows the simulation domain after meshing. The number of elements was of order 150,000 and simulations required tens of minutes to a few hours on a 2 GHz Pentium PC.

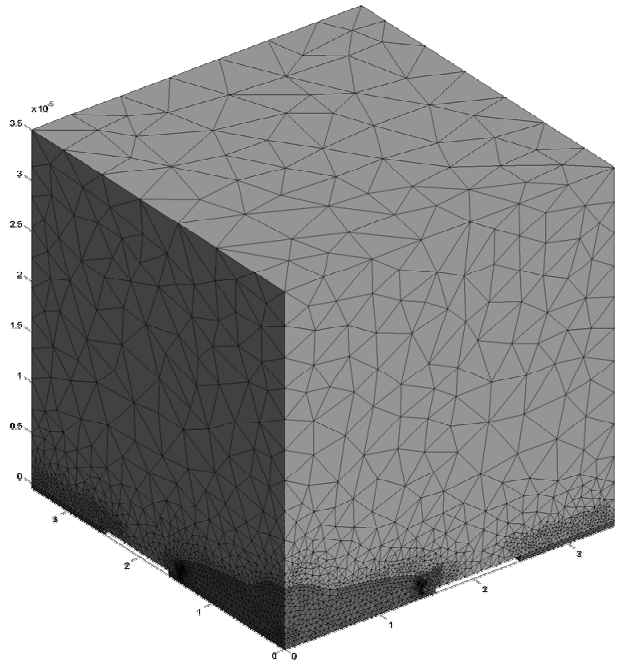

Figure 4. Simulation domain after meshing.

Representative results obtained from the simulations are presented in Figs. 5a-c. These results were obtained with a cell-electrode separation of 0.15 μm and are presented for frequencies of 1000, 10^5, and 10^7 Hz. In these figures, the colors (shading) represent the potential along surfaces. Arrows represent the direction and magnitude of the current density.

Figure 5a shows the potential and current density at 1000 Hz. At the frequency the impedance of the electrical double layer is large compared to the resistance of the medium in the cell-electrode gap. This is apparent because most of the applied potential drops across the region representing the electrical double layer. Consequently the potential of the medium at the center of the cell is nearly equal to the potential at the cell edge. Since current flows beneath the entire cell, we expect to the impedance to be essentially unchanged by the cell.

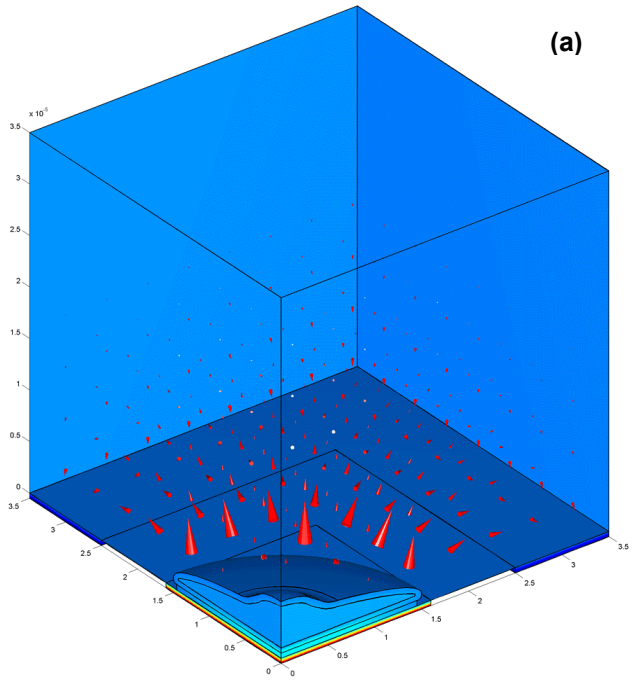

Figure 5a. Simulated electric potential (surface colors) and current density magnitude (arrows) for 1000 Hz.

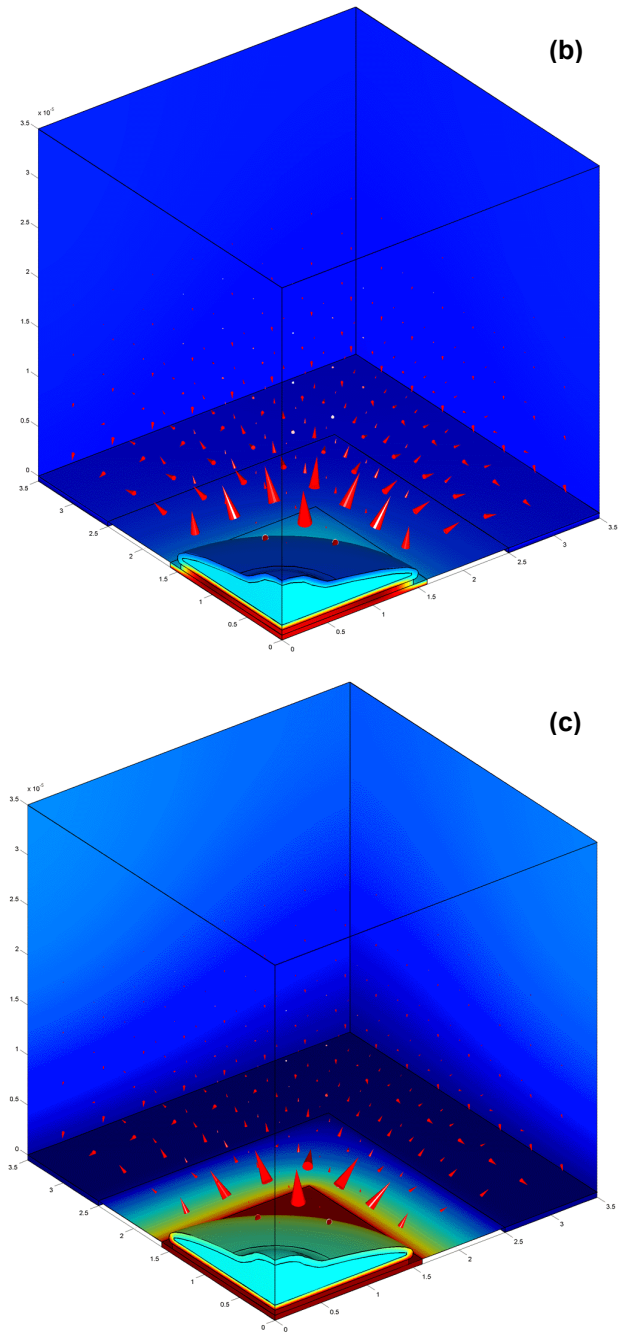

Figure 5b,c. Simulated electric potential (surface colors) and current density magnitude (arrows) at (b) 10^5 Hz and (c) 10^7 Hz.

At 10^5 Hz, the potential of the medium is nearly equal to the applied potential for most of the area under the cell (Fig. 5b). Current penetrates only a few mm from the cell edge. In this frequency range the cell blocks current from a considerable fraction of the electrode area and the impedance is strongly affected by the presence of the cell.

At very high frequencies (Fig. 5c, 10^7 Hz) the impedance of the exposed electrode area is small compared to the spreading resistance in the cell growth medium. Potential drop occurs over tens of μm around the sensing electrode. In this region the impedance is also affected by the cell but to a lesser degree; the spreading resistance depends weakly on the exposed electrode area (approximately $\sim A^{-1/2}$).

Note that in all cases the potential drop occurs mainly around the sensing electrode and not at the counterelectrode. This is the case despite the comparatively small area ratio between these two electrodes. In a measurement the counterelectrode is very large although some of that area may be covered by cells.

The simulated impedance magnitude with and without cells is shown in Fig. 6. Without cells the expected f^n behavior is observed at low frequencies and a constant impedance at high frequencies. With cells present there is no change in measured impedance at low frequencies, an increase at intermediate frequencies and a smaller increase at very high frequencies.

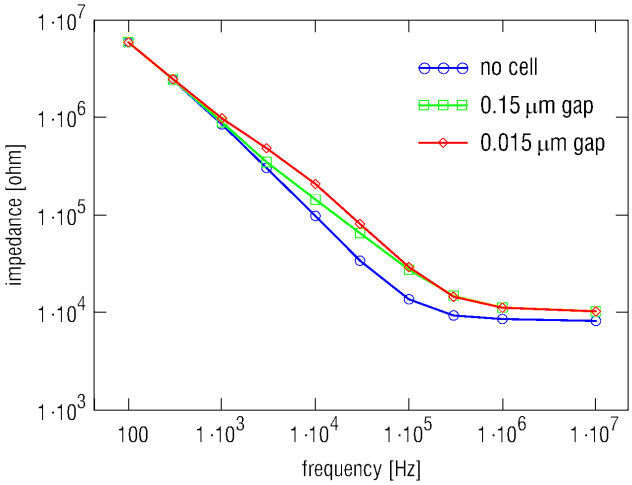

Figure 6. Impedance magnitude as a function of frequency (○) no cell (◇) 0.015 μm cell-electrode gap and (□) 0.15 μm gap.

For visualization and also for comparison with experiment it is more convenient to plot the normalized impedance change r, defined as

$$r = \frac{Z_{cell} - Z_{no\ cell}}{Z_{no\ cell}}.$$

The normalized impedance change is plotted in Figure 7. We see that the signature of cell coverage is the appearance of a peak at an intermediate frequency.

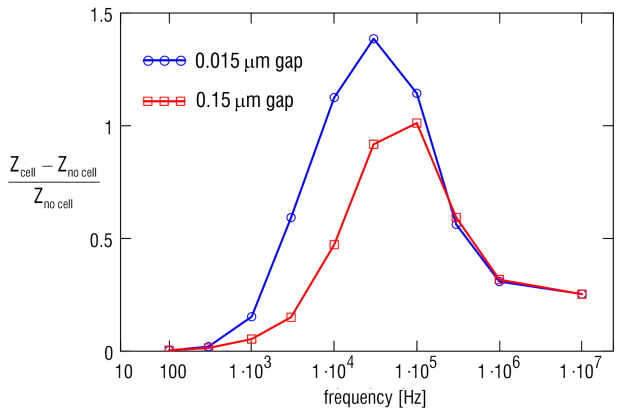

Figure 7. Normalized impedance change plotted as a function of frequency (○) 0.015 μm cell-electrode gap and (□) 0.15 μm gap.

We now discuss a graphical construction which approximately reproduces the simulation results and which can be used to gain insight into more complex geometrical situations. Figure 8 shows the equivalent circuit of the electrode with and without a cell. In these figures, $Z(\omega)$ has the f^n behavior due to the electrode double-layer impedance. Without a cell, at low frequencies the impedance follows $Z(\omega)/A$ with a slope of $-n$ on a log Z_m- log f plot as shown in Fig. 9. At high enough frequencies (above $f = f_3$) spreading resistance dominates and Z_m remains constant.

With a cell present, there are two branches which can carry current as shown in Fig. 8b, one representing the cell-covered area A_{cell} and the other the uncovered area A-A_{cell}. R_{gap} represents approximately the resistance of the medium in the cell-electrode gap.

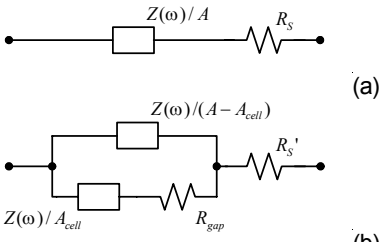

Figure 8. Equivalent circuits (a) with no cell and (b) with cell.

Following a similar analysis, Fig. 9 shows that the impedance of a partially cell-covered electrode follows $Z(\omega)/A$ at low frequencies and becomes constant at a frequency f_1 such that

$$\frac{Z(\omega_1)}{A} = R_{gap}$$

and the maximum deviation from the no-cell case occurs at f_2 such that

$$\frac{Z(\omega_2)}{A - A_{cell}} = R_{gap}.$$

The onset frequency f_1 and the peak frequency f_2 depend on the cell size and the cell-electrode gap. This is because the resistance $R_{gap} \sim (\rho r_{cell}/g)$, where ρ is the resistivity of the cell growth medium, r_{cell} is the cell radius, and γ is the cell-electrode gap. For example, the onset frequency f_1 depends on the cell radius and gap according to

$$f_1 = \left(\frac{g}{r_{cell}\,\rho} \right)^{1/2}$$

Consequently we expect the position of the cell-induced peak to provide an indication of changes of cell size or cell-electrode gap.

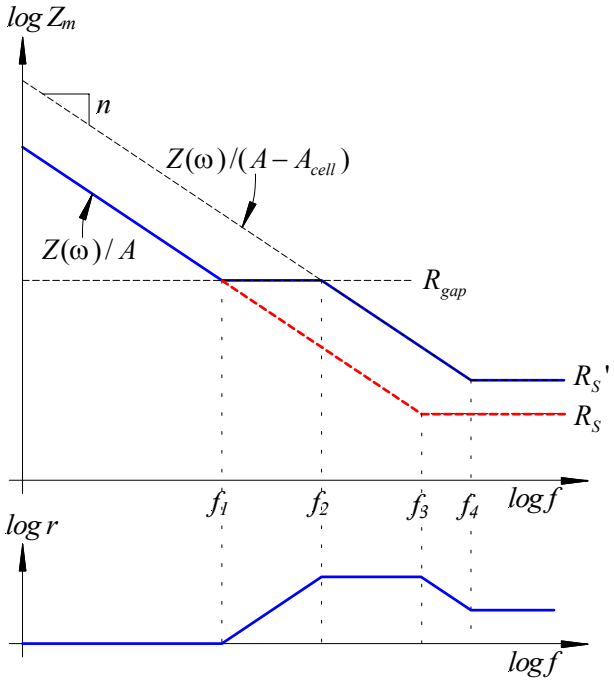

Figure 9. Construction used to understand the dependence of impedance on cell size and cell-electrode gap.

EFFECT OF FOCAL ADHESIONS AND MULTIPLE CELLS

Insight gained from our finite element simulations and the discussion above can be used to understand the influence of focal adhesions and contiguous groups of cells. We consider first the effect of focal adhesions. As noted earlier, focal adhesions provide contacts between the cell and the surface and represent a small fraction of the total cell area. Figure 10 shows an outline drawing of a cell along with a typical pattern of focal adhesions. Focal adhesions typically are between <6 μm^2 in area.

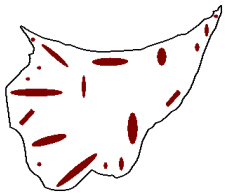

Figure 10. Cell outline showing typical pattern of focal adhesion regions.

Probably current flow will be blocked from the portion of the electrode covered by focal adhesions. This will cause only a small increase in the measured impedance, since current can flow around focal adhesion regions at low frequencies and at high frequencies current flow is blocked by the cell. Changes to the focal adhesion may have an indirect effect if the cell-electrode gap is changed [10].

Impedance measurements on larger electrodes will depend on the manner in which cells grow, that is, on whether they form continguous regions which do not pass current between cells. When there are large contiguous regions, the peak frequency will be determined by the effective radius of the contiguous region rather than the individual cell size.

ACKNOWLEDGEMENTS

This material is based upon work supported by the National Science Foundation under Grant No. ECS-0088520. Any opinions, findings, and conclusions or recommendations expressed in this material are those of the authors and do not necessarily reflect the views of the National Science Foundation.

REFERENCES

[1] Giaever, I. and Keese, C.R., "Use of electric fields to monitor the dynamical aspect of cell behavior in tissue culture," *IEEE Transactions on Biomedical Engineering*, BME-33(2):242-247 (1986).

[2] Keese, C.R. and Giaever, I., "A biosensor that monitors cell morphology with electric fields," *IEEE Engineering in Medicine and Biology Magazine*, June/July:402-408 (1994).

[3] Tiruppathi, C., Malik, A.B., Del Vecchio, P.J., Keese, C.R., and Giaever, I., "Electrical method for detection of endothelial cell shape change in real time: assessment of endothelial barrier function," *Proc. Natl. Acad. Sc*i., 89:7919-7923 (1992).

[4] Giaever, I. and Keese, C.R., "Micromotion of mammalian cells measured electrically," *Proc. Natl. Acad. Sci.*, 88:7896-7900 (1991).

[5] Wegener, J., Sieber, M. and Galla, H.J., "Impedance analysis of epithelial and endothelial cell monolayers cultured on gold surfaces," *J. Biochem. Biophys. Methods*, 32(3):151-170 (1996).

[6] Ehret, R., Baumann, W., Brischwein, M., Schwinde, A., Stegbauer, K. and Wolf, B., "Monitoring of cellular behaviour by impedance measurements on interdigitated electrode structures," *Biosensors and Bioelectronics*, 12(1):29-41 (1997).

[7] D. Nguyen , H. Xiaoqiu , T. Afentakis , M. Hatalis, M.Domach , and D. Greve, "Screening of isolated cells via arrays of impedance sensors," (paper presented at the 225th ACS National Meeting (New Orleans)/BIOT / Sci-Mix Poster, March, 2003).

[8] "The use of the Conductive Media DC Application Mode for time-harmonic problems," solution 904, support knowledge base, from htttp://www.comsol.com.

[9] M. Miskian, J.J. Kasianowicz, B. Robertson, and O. Petersons, "Frequency response of alternating currents through the Staphylococcus aureus α-hemolysin ion channel," Bioelectromagnetics 22, 487 (2001).

[10] Fibroblast Proliferation & Effect of Protein Kinase Inhibitor (H-7) Monitored in Microimpedance Sensor Arrays," Duc D. Nguyen, Xiaoqiu Huang, David W. Greve and Michael M. Domach, (submitted to Nature Biotechnology).